11th International Symposium on Turbulence and Shear Flow Phenomena (TSFP11)
Southampton, UK, July 30 to August 2, 2019

FLOW OVER A SQUARE BAR ROUGHNESS

Alexander Smits
Department of Mechanical and Aerospace Engineering
Princeton University
Princeton, NJ 08544, USA
asmits@princeton.edu

Liuyang Ding
Department of Mechanical and Aerospace Engineering
Princeton University
Princeton, NJ 08544, USA
liuyangd@princeton.edu

Tyler Van Buren
Department of Mechanical and Aerospace Engineering
Princeton University
Princeton, NJ 08544, USA
tburen@princeton.edu

ABSTRACT

The response and recovery of a turbulent pipe flow perturbed by a single square bar roughness element were studied using particle image velocimetry. The flow was fully developed upstream of the perturbation, and the Reynolds number based on the bulk velocity and the pipe diameter was 156,000. Measurements were conducted with two bar heights, h/D = 0.05 and 0.1 (h is the bar height; D the pipe diameter), over a distance up to $100h$ downstream. The reattachment lengths of the small and large bars were $8.18h$ and $9.41h$, respectively, which are longer compared to flows over a backward-facing step with similar Reynolds numbers and expansion ratios. For the small bar the mean velocity in the center region remained higher than for the equilibrium profile throughout the measurement domain, but the opposite was true for the large bar as a consequence of a higher rate of turbulent transport. The bar height was shown to be the correct length scale for the near-field flow behavior, while in the far field the pipe radius was the correct scale for the recovery process. For both bar sizes, the flow at $100h$ downstream of the perturbation was still far from the equilibrium state, and the slow variation implied a long-lasting recovery behavior beyond that point.

INTRODUCTION

High Reynolds number turbulent flows subjected to abrupt changes in surface conditions, such as changes in surface roughness and the presence of steps on the surface, represent a class of perturbed or non-equilibrium flows. Such flows have been largely overlooked in recent years, despite the fact that they represent conditions commonly encountered in flows over large vehicles such as ships and submarines. The behavior of such flows is often complex, and typically not captured by Reynolds-averaged Navier-Stokes (RANS) methods. In addition, there is almost no data to show their dependence on Reynolds number, and understanding such flows may inspire novel methods of flow control.

Past studies have revealed some intriguing aspects of this class of flows. First, abrupt changes can cause long-lasting changes in turbulent structure. For example, Smits *et al.* (1979) investigated a flow exposed to a short region of concave curvature, and found that the flow displayed an initial amplification of the Reynolds stresses, followed by a rapid decay. Surprisingly, the decay was not monotonic in that the Reynolds shear stress in the outer region fell to levels below the equilibrium values. The authors attributed the pronounced second-order response to the interaction between the shear stress and the mean shear, which is in effect not peculiar to curved flows. For example, a similar response was seen in the recovery from a step change in surface roughness from rough to smooth by Antonia & Luxton (1972) and Van Buren *et al.* (2019). Most notable was that the long-lasting collapse of the Reynolds stresses appears as the result of an impulse in *destabilizing* curvature (Hoffmann *et al.*, 1985), a rather unexpected outcome that is well beyond the capacity of RANS models.

Second, the overshoot in flow response suggests that such abrupt changes may be used as a form of passive flow control. For example, if the flow exhibits a long region of lower skin friction in response to an abrupt change in surface characteristic, then it may be possible that by periodically initiating abrupt changes in a wall-bounded flow the overall response may lead to lower turbulence levels and a reduced drag. This possibility has never before been explored.

Third, forward and backward facing steps are often encountered in practical flows. For large backward facing steps a considerable amount of work has been done to study the characteristics of the separation bubble and the initial flow recovery (large steps are defined by having $h/\delta_0 \gg 1$, where δ_0 is the boundary layer thickness at the step) (Bradshaw & Wong, 1972; Vogel & Eaton, 1985; Simpson, 1989). Small steps ($h/\delta_0 \ll 1$), however, have received limited attention despite being common in application – such as when there are mismatches in height in the piece-wise rubber coatings used on submarines. Small steps can have significant effects on drag, where they behave like isolated roughness elements (Jiménez, 2004), and produce noise (Ji & Wang, 2010).

In the present work, we conducted experiments on the response to a single square bar roughness element, using two different sizes of $h/D = 0.05$ and 0.10. The experiments were performed using fully-developed pipe flow (diameter D) as the inflow boundary condition. This setup was chosen because: (1) all aspects of the upstream and far-downstream conditions are known in detail; (2) all boundary conditions are well defined, making it ideal for testing and developing RANS and other turbulence models; (3) momentum balances can be used to derive the wall friction evolution (which is very difficult to do accurately in boundary layer studies); and (4) the inflow is fully-developed, thus the evolution downstream of a wall modification can be studied by moving the perturbation rather than moving the measurement location.

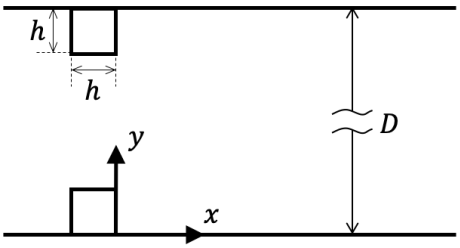

Figure 1: Axial-radial slice of the test section. Two bar sizes were tested: $h/D = 0.05$ and 0.10. Flow is from left to right.

EXPERIMENT

The experiment was conducted in a recirculating pipe facility with water being the working fluid. The pipe had an inner diameter of $D = 38.1$ mm, and upstream of the perturbation the flow developed over a length of approximately $200D$ to ensure a fully developed inflow condition. The perturbation was introduced axisymmetrically by a square-cross-section ring, which was held in position by friction. The cross-sectional geometry of the ring and the coordinate system are illustrated in figure 1: x is the axial direction, y is the wall-normal direction, and the origin is at the corner formed by the pipe wall and the downstream face of the square bar. The upstream fully developed flow had a Reynolds number ($Re_D = U_b D/\nu$) of approximately 156,000, where $U_b \approx 4.1$ m/s is the bulk velocity and $\nu = 10^{-6}$ the kinematic viscosity of water at 20 °C. From the friction factor correlation reported by McKeon *et al.* (2004), the upstream friction velocity $u_\tau = 0.186$ m/s, and $Re_\tau = u_\tau R/\nu = 3550$ ($R = D/2$ is the pipe radius). The Reynolds number based on the square bar height and the upstream bulk velocity, i.e. $Re_h = U_b h/\nu$, is 15600 for $h/D = 0.1$ and 7800 for $h/D = 0.05$. The linear expansion ratio, $ER = D/(D-2h)$, is 1.25 and 1.11 in our measurements.

We conducted planar particle image velocimetry (PIV) in the streamwise-wall-normal plane to study the response and recovery of the flow. PIV data were taken at multiple streamwise locations covering a distance of $100h$ downstream of the perturbation. At each streamwise location, the camera (LaVision Imager sCMOS) was positioned to achieve a magnification of 0.32 (49 pix/mm). The laser light sheet was orientated so that its propagation direction had a 45° angle with respect to the y-axis, which allowed us to filter out reflections from the glass pipe wall using a polarizing filter.

For each streamwise location, 10,000 image pairs were recorded and processed to calculate mean statistics. Correlation-based PIV interrogation was performed using an in-house code featuring symmetric iterative image deformation (Scarano & Riethmuller, 2000). The final interrogation spot size was 32×32 pixels with 50% overlap, corresponding to a spatial resolution of 0.65 mm with a 0.33 mm data spacing.

RESULTS

Reattachment

Mean streamlines were computed by integrating the time-averaged velocity field. The results are presented in figure 2, where the separation and the primary recirculating zone are clearly seen. The strong shear layer lying between the upper flow and the separation bubble is indicated by the negative (blue) vorticity region. In the corner formed by the downstream face of the square bar and the pipe wall, the positive vorticity (counterclockwise) implies the existence of a secondary bubble, albeit it is not resolved by the streamlines due to the limited resolution of the PIV measurement. It is also noticed that the highest point of the separation bubble slightly exceeds the height of the square bar, resulting in mildly converged streamlines upstream of the center of the bubble. The streamlines then diverge and split near the mean reattachment point. This behavior is consistent with pressure data reported in numerical studies (e.g. Leonardi *et al.* (2003)) – the flow starts experiencing an adverse pressure gradient only downstream of the center of the separation bubble.

Figure 3 shows the mean axial velocity U (hereafter, we use Reynolds decomposition, $u = U + u'$) as a function of x/h at $y/D = 0.0086$, the first grid point away from the wall in our PIV measurement. For both cases, the backflow near the wall reaches its maximum velocity at approxi-

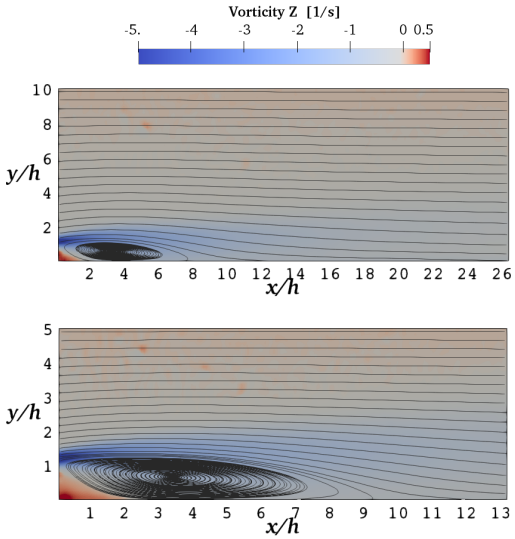

Figure 2: Mean streamlines superimposed on the vorticity field showing the primary separation bubble, the secondary bubble (red) and the reattachment location. Top: $h/D = 0.05$; bottom: $h/D = 0.1$. Shown is the lower half of the pipe.

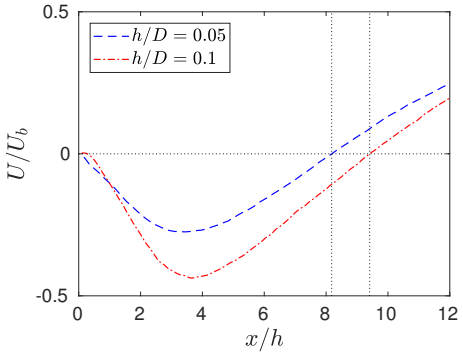

Figure 3: Mean axial velocity U at $y/D = 0.0086$. The dotted cross lines indicate the reattachment location $x_r/h = 8.18$ and 9.41 for $h/D = 0.05$ and 0.1, respectively.

mately halfway along the separation bubble, and then decreases to zero. The mean reattachment location, x_r, is then determined as the zero-crossing of each curve. For $h/D = 0.05$ and 0.1, $x_r/h = 8.18$ and 9.41, respectively.

For reattachment lengths of separated flows, past studies have focused mainly on the behavior of boundary layer flows over backward-facing steps. Relatively fewer studies have examined the response of internal flows perturbed by small wall-mounted obstacles, as in the present study. There are at least two parameters relevant to both geometries, that is, Re_h and the expansion ratio (ER). Jovic & Driver (1995) conducted experiments on backward-facing step flows with $Re_h = 5000 \sim 37500$ and ER similar to ours, and found $x_r/h = 5.35 \sim 6.90$ for all their cases, noticeably shorter than the present results. Adams & Johnston (1988) reported measurements for a backward-facing step with $ER = 1.25$ and $Re_h = 7650 \sim 41000$, and similarly found shorter reattachment lengths ($x_r/h = 6.07 \sim 6.80$). These comparisons suggest that the different upstream flow history arising from different geometries plays an important role in determining the reattachment length. At least when ER is in the range of the current study (approximately 1.1∼1.25), the sudden contraction and expansion of the incoming flow imposed by the square bar element appears to lead to a longer reattachment distance. For larger ER, however, Dimaczek *et al.* (1989) found x_r is shorter compared to that of a backward-facing step, which was explained by the authors as an effect of the strong flow separation at the leading edge.

Recovery

Downstream of the reattachment region, the recovery process is determined by the interaction between the mean velocity field and the turbulence field through turbulence production, dissipation and transport. Figure 4 compares the mean axial velocity field for the two bar sizes, and the turbulence fields $\overline{u'u'}$ and $-\overline{u'v'}$ are compared in figure 5 and 6. As clearly seen from the velocity fields, immediately after the bar, the stronger contraction by the large bar creates a higher velocity gradient near $y = h$. This higher velocity gradient produces more turbulence, which is evident in the $\overline{u'u'}$ and $-\overline{u'v'}$ fields. As the flow moves downstream, the momentum exchange ($-\overline{u'v'}$) between the high- and low-speed layers attenuates the velocity differences. Figure 6 shows that the momentum exchange rate is higher for the large bar, which explains that the velocity distribution in the y-direction, $U(y;x)$, flattens more rapidly for $h/D = 0.1$, as seen in figure 4.

To further examine the flattening of $U(y;x)$ and its recovery back to the fully developed state, the velocity profiles at far downstream locations, $x/h = 60$, 80 and 100, are plotted in figure 7 for both bar sizes. The differences between the two cases are distinct – for $h/D = 0.05$, the velocity near the center at $x/h = 60$ is about 10% above the fully developed profile, and it decreases only slightly (∼3%) by the time the flow reaches $x/h = 100$. In contrast, the velocity profiles of $h/D = 0.1$ seem to be over flattened by $-\overline{u'v'}$ so that the flow moves more slowly near the center and faster near the wall compared to the fully developed flow. The centerline velocity is about 12% below the fully developed value, and, again, it varies only slightly from $x/h = 60$ to 100. This observation implies an undershoot behavior of the mean velocity for $h/D = 0.1$, as it needs eventually to return to its equilibrium state. Such a second-order response is similar to that observed in a variety of flows undergoing recovery after perturbation (e.g. Smits *et al.* (1979)). What is the most striking results shown in figure 7 is that the flow is not yet recovered to equilibrium even $100h$ downstream of the perturbation, and the slow variation from $x/h = 60$ to 100 implies the recovery process will continue for a long distance further downstream.

As indicated earlier, the Reynolds shear stress is responsible for the different recovery behaviors of the velocity profile. In the $-\overline{u'v'}$ field shown in figure 6, besides the intensity, what is also noticeably different is the diffusion of the turbulence. For $h/D = 0.05$, the high-turbulence region shifts towards the centerline with increasing width and decreasing peak intensity. This diffusion process is confined to the region $y < R$ for at least $x/h \leq 100$. The diffusion process for $h/D = 0.1$ is qualitatively similar, but the rate of expansion of the high-turbulence region is much faster. As indicated in figure 6, high levels of $-\overline{u'v'}$ reach the centerline at approximately $x/h = 30$, merging and mixing with the contributions from the other parts of the pipe. As a result, the flattening of the velocity distribution is more pronounced for $h/D = 0.1$, especially near the pipe centerline.

We can examine the transport of $-\overline{u'v'}$ in a more quantitative way by inspecting the radial location of the maximum value of $-\overline{u'v'}$, that is, y_M, as a function of x/h. This is presented in figure 8. For both cases, y_M starts close to $y = h$ and stays relatively flat until $x/h = 10$. Between $x/h = 10$ and 30, y_M for both cases exhibits a power-law behavior approaching the centerline with the same power of approximately 0.6, that is, $y_M = \alpha(x/h)^{0.6}$ for $10 \leq x/h \leq 30$, where α is a constant of proportionality. When y_M is scaled with R as plotted in figure 8(a), α is 0.26 for $h/D = 0.1$ and 0.12 for $h/D = 0.05$. This is to say, when the comparison is based on the same length scale (R in this case), the transport of $-\overline{u'v'}$ in $10 \leq x/h \leq 30$ takes place more than twice as fast for $h/D = 0.1$ than for $h/D = 0.05$. Downstream of the power-law range, the high-turbulence region diffuses into the centerline for the $h/D = 0.1$ case, and thus y_M is level at $y/R \approx 0.5$ until $x/h \approx 70$. Further downstream, $-\overline{u'v'}$ near the centerline gets dissipated so that the peak of $-\overline{u'v'}$ shifts towards the wall approaching an equilibrium state. On the other hand, y_M for $h/D = 0.05$ continues to grow over the distance $30 \leq x/h \leq 100$.

When y_M is scaled with h, as is done in figure 8(b), we immediately achieve a collapse of the data for $x/h \leq 30$. The collapse suggests that the bar height, h, is the correct length scale for describing the turbulent behaviors in the near field. Far downstream, the pipe radius comes into effect and interferes with the established length scale. The length scale for the far-field recovery behavior is expected to be R, but confirmation will require more far-field data.

Since h is not the only length scale for the turbulent recovery far downstream of the perturbation, the recovery of $-\overline{u'v'}$ is also quite different for the two cases at the same normalized downstream distance (x/h). Figure 9 shows the profiles of $-\overline{u'v'}$ at $x/h = 80$ and 100. In the $h/D = 0.05$ case, $-\overline{u'v'}$ significantly exceeds the fully developed profile with its peak located around $y/R = 0.4$ at $x/h = 80$. The peak decreases by about 20% and shifts to $y/R = 0.5$ at $x/h = 100$, which is a result of $-\overline{u'v'}$ being transported towards the centerline, as discussed earlier. For $h/D = 0.1$, $-\overline{u'v'}$ in the region $0.3 < y/R < 1$ drops sharply between $x/h = 80$ and 100, while the near-wall values stays high and are relatively unachanged. The collapse below the fully developed profile again suggests a second-order response of the recovery process. Further recovery will need to rely on the turbulence production surpassing the dissipation in the

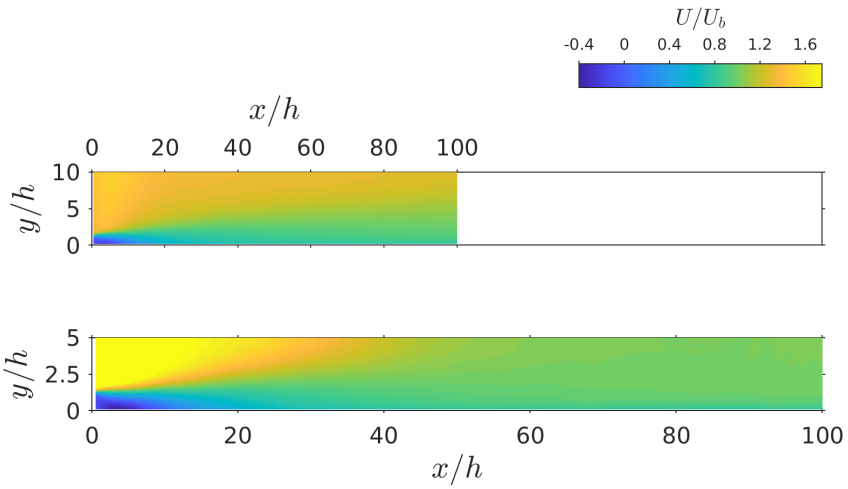

Figure 4: Comparison of U/U_b for $x/h = 0 \sim 100$. Top: $h/D = 0.05$; bottom: $h/D = 0.1$. Shown is the lower half of the pipe.

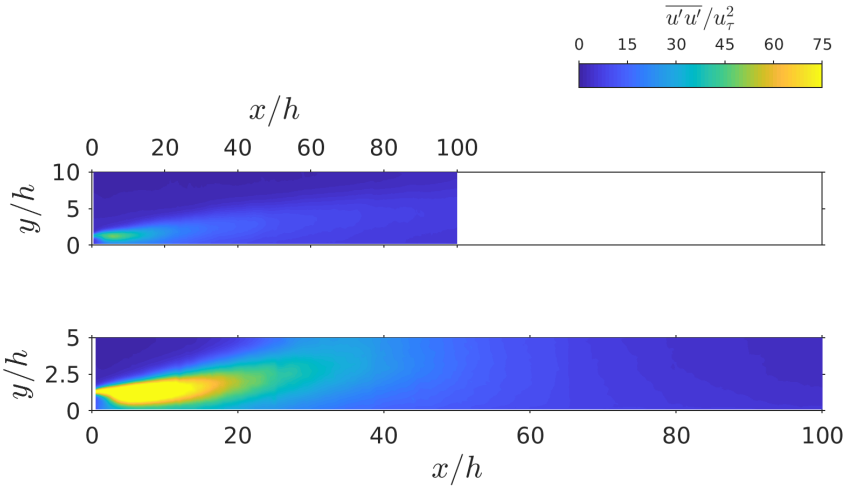

Figure 5: Comparison of $\overline{u'^2}/u_\tau^2$ for $x/h = 0 \sim 100$. Here (and in subsequent figures) u_τ is the friction velocity of the upstream fully developed flow. Top: $h/D = 0.05$; bottom: $h/D = 0.1$. Shown is the lower half of the pipe.

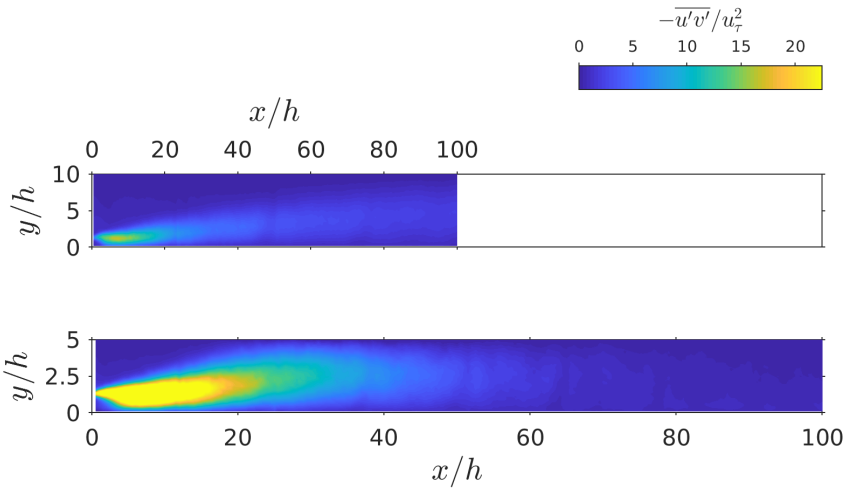

Figure 6: Comparison of $-\overline{u'v'}/u_\tau^2$ for $x/h = 0 \sim 100$. Top: $h/D = 0.05$; bottom: $h/D = 0.1$. Shown is the lower half of the pipe.

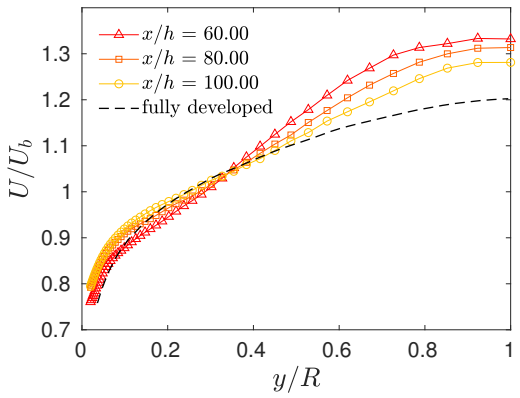

(a) $h/D = 0.05$

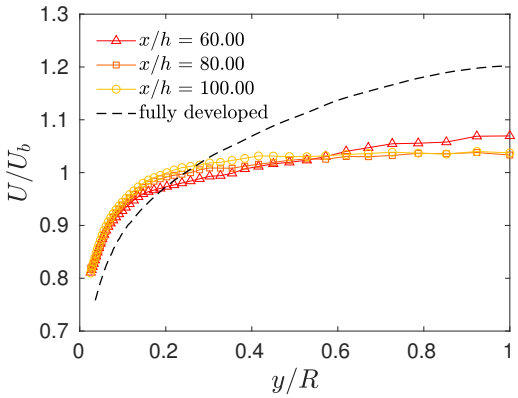

(b) $h/D = 0.1$

Figure 7: Recovery of the mean velocity.

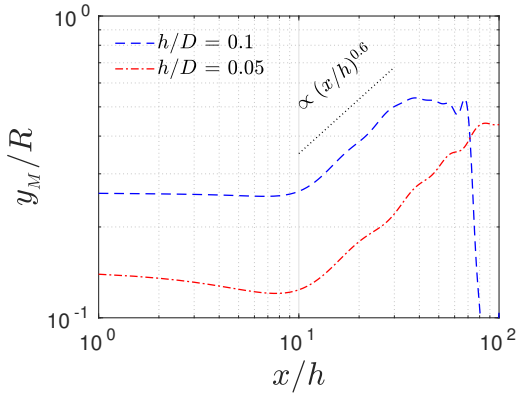

(a) y_M scaled with R

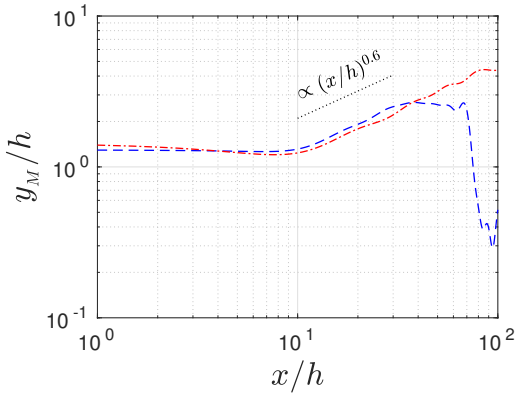

(b) y_M scaled with h

Figure 8: The location of maximum Reynolds shear stress, y_M, as a function of x/h. The $(x/h)^{0.6}$ line indicates a power-law behavior of turbulent diffusion.

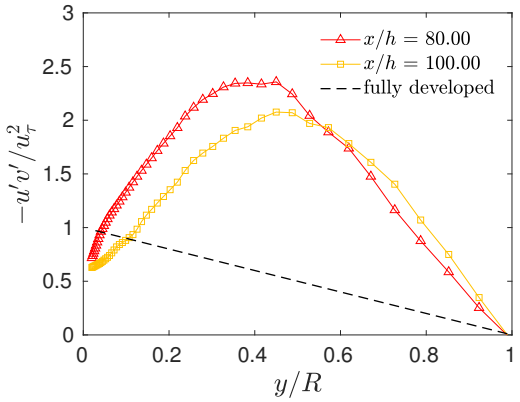

(a) $h/D = 0.05$

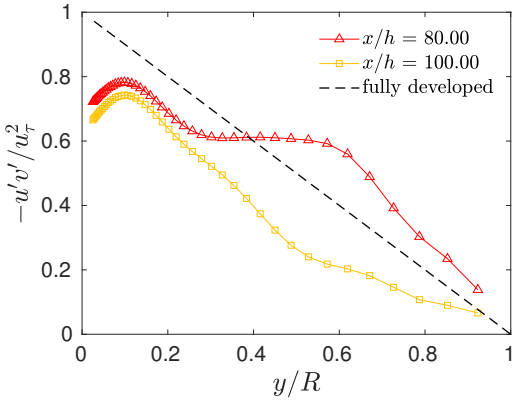

(b) $h/D = 0.1$

Figure 9: Recovery of the Reynolds shear stress, normalized by u_τ^2 of the upstream fully developed flow

near-wall region, as the wall remains to be the only forcing mechanism for the long-lasting recovery process. The excess near-wall turbulence will most likely then be transported away from the wall to drive the evolution to the equilibrium state.

CONCLUSIONS

We experimentally investigated a fully developed turbulent pipe flow perturbed by a single square bar roughness element mounted on the wall of the pipe. Two bar heights, $h/D = 0.05$ and 0.1, were used. PIV was carried out to measure the mean velocity and Reynolds stresses for a downstream distance of $100h$.

The reattachment lengths were found to be $8.18h$ and $9.41h$ for the small and large bars, respectively. These values are larger than those found in studies of backward-facing steps with similar Re_h and ER, implying the upstream flow history plays an important role in the physics of reattaching flows.

The turbulence arising from the square-bar perturbation was more intense for the $h/D = 0.1$ case, and so was the rate of turbulent transport. The strong transport by $-\overline{u'v'}$ over-flattened the velocity profile for $h/D = 0.1$, whereas the velocity profile of the $h/D = 0.05$ case exhibited a higher gradient in the wall-normal direction at $x/h = 100$ compared to the equilibrium state.

The transport of the Reynolds shear stress for the two cases were shown to follow the same power law (power of 0.6) in the near field ($x/h \leq 30$) when scaled with h. The collapse suggested h to be the correct length scale for the near-field turbulent behaviors. Further downstream, the transport of turbulence was affected by the geometric constraint imposed by the pipe radius. As a result, the $-\overline{u'v'}$ profile at $x/h = 100$ for the two cases displayed significant differences.

The profiles of U and $-\overline{u'v'}$ at $x/h = 100$ showed that the flow had not yet recovered to the fully developed state. The slow variation from $x/h = 80$ to 100 implied a long-lasting recovery behavior. A second-order response was also discovered for $h/D = 0.1$.

Acknowledgments

The authors gratefully acknowledge the support under ONR Grant "Understanding Turbulence on Navy Vehicles" N00014-17-1-2309 (Program Manager Joseph Gorski).

REFERENCES

Adams, E. W. & Johnston, J. P. 1988 Effects of the separating shear layer on the reattachment flow structure. Part 2: Reattachment length and wall shear stress. *Experiments in Fluids* **6** (7), 493–499.

Antonia, R. A. & Luxton, R. E. 1972 The response of a turbulent boundary layer to a step change in surface roughness. Part 2. Rough-to-smooth. *J. Fluid Mech.* **53** (04), 737–757.

Bradshaw, P. & Wong, F. Y. F. 1972 Reattachment and relaxation of a turbulent shear layer. *J. Fluid Mech.* **52**, 113–135.

Dimaczek, G., Tropea, C. & Wang, A.-B. 1989 Turbulent flow over two-dimensional, surface-mounted obstacles: plane and axisymmetric geometries. In *Advances in Turbulence 2*, pp. 114–121. Springer.

Hoffmann, P. H., Muck, K. C. & Bradshaw, P. 1985 The effect of concave surface curvature on turbulent boundary layers. *J. Fluid Mech.* **161**, 371–403.

Ji, M. & Wang, M. 2010 Sound generation by turbulent boundary-layer flow over small steps. *J. Fluid Mech.* **654**, 161–193.

Jiménez, J. 2004 Turbulent flows over rough walls. *Annu. Rev. Fluid Mech.* **36**, 173–196.

Jovic, S. & Driver, D. 1995 Reynolds number effect on the skin friction in separated flows behind a backward-facing step. *Experiments in Fluids* **18** (6), 464–467.

Leonardi, S., Orlandi, P., Smalley, R. J., Djenidi, L. & Antonia, R. A. 2003 Direct numerical simulations of turbulent channel flow with transverse square bars on one wall. *J. Fluid Mech.* **491**, 229–238.

McKeon, B. J., Swanson, C. J., Zagarola, M. V., Donnelly, R. J. & Smits, A. J. 2004 Friction factors for smooth pipe flow. *J. Fluid Mech.* **511**, 41–44.

Scarano, F. & Riethmuller, M. L. 2000 Advances in iterative multigrid PIV image processing. *Experiments in Fluids* **29** (1), S051–S060.

Simpson, R. L. 1989 Turbulent boundary-layer separation. *Annu. Rev. Fluid Mech.* **21** (1), 205–232.

Smits, A. J., Young, S. T. B. & Bradshaw, P. 1979 The effect of short regions of high surface curvature on turbulent boundary layers. *J. Fluid Mech.* **94** (2), 209–242.

Van Buren, T., Hellström, L. H. O. & Smits, A. J. 2019 Turbulent pipe flow response to rough-to-smooth step change in roughness: flow structure. In *Proc. Turbulence and Shear Flow Phenomena 11*. University of Southampton, Southampton, UK.

Vogel, J. C. & Eaton, J. K. 1985 Combined heat transfer and fluid dynamic measurements downstream of a backward-facing step. *Journal of Heat Transfer* **107** (4), 922–929.